Numerical simulation of interlaminar damage propagation in CFRP cross-ply laminates under transverse loading

Masaaki Nishikawa [a], Tomonaga Okabe [b,*], Nobuo Takeda [c]

[a] *Department of Aeronautics and Astronautics, School of Engineering, The University of Tokyo,*
c/o Transdisciplinary Sciences Bldg. Mailing Box 311, 5-1-5 Kashiwanoha, Kashiwa-shi, Chiba 277-8561, Japan
[b] *Department of Aerospace Engineering, Tohoku University, 6-6-01 Aoba-yama, Aoba-ku, Sendai 980-8579, Japan*
[c] *Department of Advanced Energy, Graduate School of Frontier Sciences, The University of Tokyo,*
c/o Transdisciplinary Sciences Bldg. Mailing Box 302, 5-1-5 Kashiwanoha, Kashiwa-shi, Chiba 277-8561, Japan

Abstract

This paper proposes a numerical simulation of interlaminar damage propagation in FRP laminates under transverse loading, using the finite element method. First, we conducted drop-weight impact tests on CFRP cross-ply laminates. A ply crack was generated at the center of the lowermost ply, and then a butterfly-shaped interlaminar delamination was propagated at the 90/0 ply interface. Based on these experimental observations, we present a numerical simulation of inter-laminar damage propagation, using a cohesive zone model to address the energy-based criterion for damage propagation. This simulation can address the interlaminar delamination with high accuracy by locating a fine mesh near the damage process zone, while maintaining computational efficiency with the use of automatic mesh generation. The simulated results of interlaminar delamination agreed well with the experiment results. Moreover, we demonstrated that the proposed method reduces the computational cost of the simulation.
© 2006 Elsevier Ltd. All rights reserved.

Keywords: Composite material; Finite element method; Delamination; Cross-ply laminate; Transverse loading

1. Introduction

Composite structures composed of carbon fiber reinforced plastics (CFRP) laminates have recently been put into practical use by the aerospace industry, because of the weight saving of the structural components. However, CFRP laminates tend to suffer from internal damage, such as ply cracks and delaminations between the plies, even under a much lower load than the final failure load. In particular, since the interlaminar fracture toughness of the laminate is inferior to its in-plane fracture toughness, interlaminar delamination between the plies with different fiber orientations is easily induced by transverse loading to the laminate (Fig. 1). Interlam-
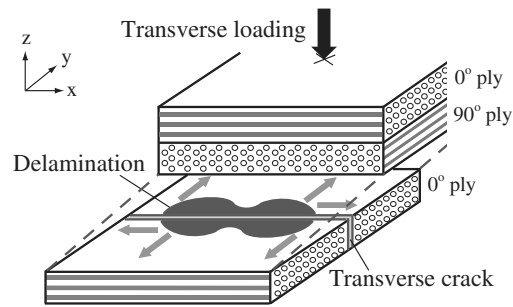
Fig. 1. Typical damage pattern of cross-ply laminate under transverse loading.

inar delamination causes severe reduction of the compressive strength of the laminate (Abrate, 1991). Therefore, a methodology to predict the generation and propagation of such an internal damage must be developed to ensure the safety and durability of these composite structures.

Numerous studies have been conducted to investigate the propagation mechanism of interlaminar delamination under transverse loading (Liu et al., 1993; Collombet et al., 1998; Geubelle and Baylor, 1998; Johnson et al., 2001; Li et al., 2002; Borg et al., 2004). Most of these studies claim that the propagation of such interlaminar delamination can be characterized by an energy-based criterion of fracture mechanics. In particular, Geubelle and Baylor (1998) contributed to the development of a simulation technique for understanding impact-induced multiple damages and the damage interaction. They applied finite element analysis combined with cohesive elements to two-dimensional transverse impact problem. They demonstrated that their method was effective for simulating the initiation and propagation of such impact-induced damages. This cohesive element method can address arbitrary paths of damage propagation between solid elements in finite element analysis, while considering an energy-based fracture criterion. Thus, it attracted considerable attention as a powerful technique for simulating the damage propagation of composite laminates (Johnson et al., 2001; Borg et al., 2004). However, these cohesive elements, which represent a softening response in the damage process, invoke numerical difficulties involved in the convergence and stabilization of nonlinear analysis (Alfano and Crisfield, 2001). Therefore, a stable solution strategy must be devised for applying the cohesive element method to obtain an accurate and quantitative prediction of damage propagation in the laminates.

To this end, we recently formulated a cohesive element based on Dugdale's cohesive zone model (Dugdale, 1960), and verified its numerical stability and consistency with the conventional fracture mechanics in the two-dimensional case (Okabe et al., 2006). This type of cohesive element is well applicable to the simulation of three-dimensional damage propagation under transverse loading. In the application, the finite element mesh used in the simulation must be carefully configured, in order to address the damage process zone of the internal damage and the geometrically nonlinear deformation due to flexure of the laminate during loading. Thus, the computational cost tends to increase when we conduct such a damage propagation simulation with a three-dimensional finite element model. Reducing computational cost must therefore also be investigated.

To solve these problems, this paper proposes an accurate and efficient numerical simulation of interlaminar damage propagation in CFRP cross-ply laminates under transverse loading, using a cohesive element method and an updating-element technique. First, we conduct low-velocity impact tests on CFRP cross-ply laminates and observed the internal damage in the laminates after the impact. Next, we present a numerical simulation to reproduce the observed damage pattern in the laminates. The effectiveness of the proposed simulation is highlighted by comparing the simulated interlaminar damage propagation with the experimental results.

2. Experiments

We conducted low-velocity impact tests on CFRP cross-ply laminates and observed the internal damage in the laminates after the impact. The tested plates were made of CFRP T800H/3631 (Toray Industries, Inc.). Their stacking sequence was $[0_4/90_2/0_4]$. Fig. 2 illustrates the dimensions of the tested plates. The drop-weight impact testing machine used in the test, developed at AIST, allowed control of the initial height of the pro-
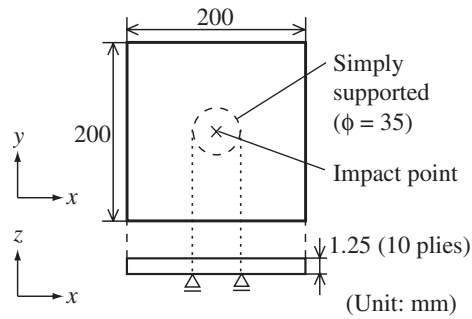
Fig. 2. Dimensions of the plate used in the low-velocity impact test.

jectile. The machine had a steel projectile with a hemispherical end (7 mm in diameter). The projectile weighed 1 kg. We used the machine to apply the point-impact load at the center of the plates, for a range of impact energy from 1 J to 5 J. The tested plates were placed on the support plate of the machine. The support plate had an open hole (35 mm in diameter) at its center. Thus, the tested plate was simply supported on the edge of the open hole. These tests were conducted at room temperature in air.

After the impacts over a range of 1 J to 3 J, a long crack along the fiber direction in the unimpacted 0° ply was observed at the surface of the plate. As the impact energy increased (4 J and 5 J), a number of short cracks
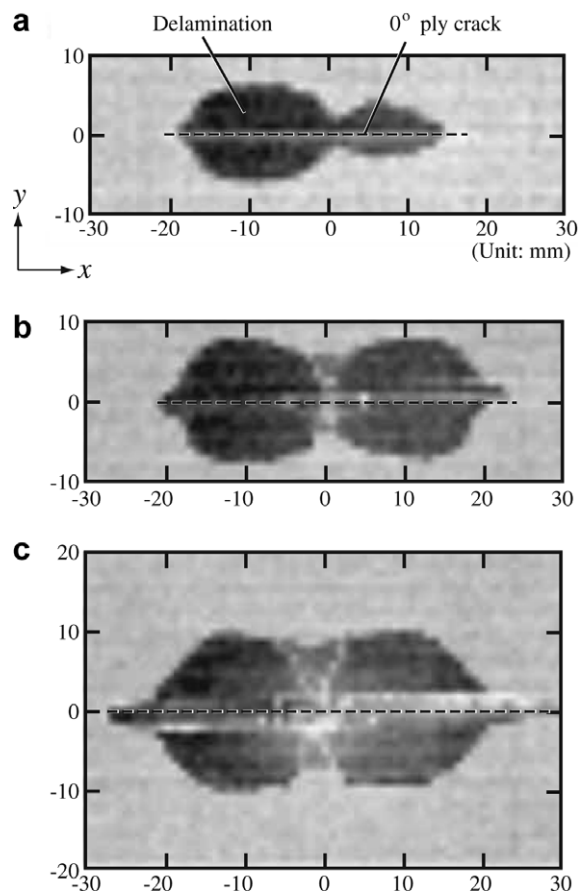

Fig. 3. Ultrasonic scanning images of the delamination in cross-ply laminates after impact: (a) after 1 J impact, (b) after 2 J impact and (c) after 3 J impact.

were generated near the long central crack. Fiber fracture was also observed at the impact point. Fig. 3 presents ultrasonic scanning images of the interlaminar delamination in the laminates after the impact. A butterfly-shaped interlaminar delamination was observed at the 90/0 lower interface of the laminates. The delaminated area was enlarged with increasing impact energy.

3. Simulation procedure

This section describes the damage propagation simulation based on finite element analysis for internal damage (0° ply crack and interlaminar delamination), for a range of low-velocity impact energy from 1 J to 3 J. Since the impact duration is long enough due to the low-velocity impact, the inertial effect on the interlaminar damage propagation is negligible as the previous literature points out (Abrate, 1991). Thus, the present simulation employs a static analysis to address this low-velocity impact.

Considering symmetry, the present simulation uses a one-quarter model in Fig. 4. The dimensions of the model are presented in Fig. 2. Each ply is modeled by a homogeneous orthotropic-elastic body and divided into three-dimensional solid elements. To simulate the propagation of the ply crack at the center in the lowermost 0° ply and interlaminar delaminations at the ply interfaces, cohesive elements are incorporated between solid elements at the corresponding positions.

Here, the cohesive elements are interface elements that relate the relative displacement between solid elements $\mathbf{\Delta}$ and the traction force per unit area $\mathbf{T}$, as shown in Fig. 5(a). This simulation addresses the relation between relative displacement and traction as illustrated in Fig. 5(b) and (c). This element acts as a penalty element maintaining the continuity of the displacements between the solid elements, while the interface between the solid elements is intact. When the traction reaches its maximum value $T_{i,\mathrm{max}}(i = \mathrm{I, II, III})$, it remains constant in the damage process zone, based on Dugdale's assumption (Dugdale, 1960) that the traction on the crack surface is uniform. Assuming that the traction is unloaded when the energy release rate reaches its critical value G_{ic} $(i = \mathrm{I, II, III})$ with increasing relative displacement, the critical relative displacement Δ_{ic} $(i = \mathrm{I, II, III})$ is defined as

$$\Delta_{ic} = \frac{G_{ic}}{T_{i,\mathrm{max}}} + \frac{T_{i,\mathrm{max}}}{2k_1} \tag{1}$$

where k_1 denotes the initial gradient in the relation of the cohesive element. When the damage process is in progress under a mixed-mode stress state, the final energy criterion is redefined as

$$D \equiv \left(\frac{\Delta_{\mathrm{I}}}{\Delta_{\mathrm{Ic}}}\right)^2 + \left(\frac{\Delta_{\mathrm{II}}}{\Delta_{\mathrm{IIc}}}\right)^2 + \left(\frac{\Delta_{\mathrm{III}}}{\Delta_{\mathrm{IIIc}}}\right)^2 = 1 \tag{2}$$

When the absolute value of relative displacement decreases in the damage process zone, elastic-unloading is considered by setting the initial gradient k_1. We call this cohesive element as the Dugdale cohesive element.

Here, we briefly describe the motivations and background for using the Dugdale cohesive element in the present simulation. We found that the calculated results with a certain bi-linear cohesive element, using the coarse finite element mesh, significantly differ from those of fracture mechanics even for the simplest problem of mode-I single-crack growth and the tangent stiffness matrix for calculation in the implicit finite element
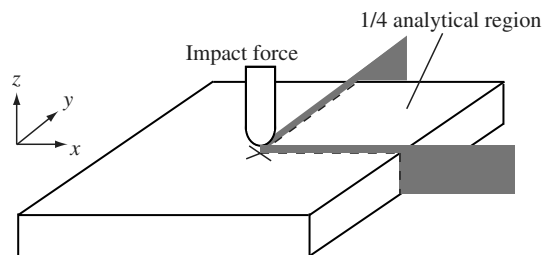

Fig. 4. Analytical model for the cross-ply laminate under transverse loading.
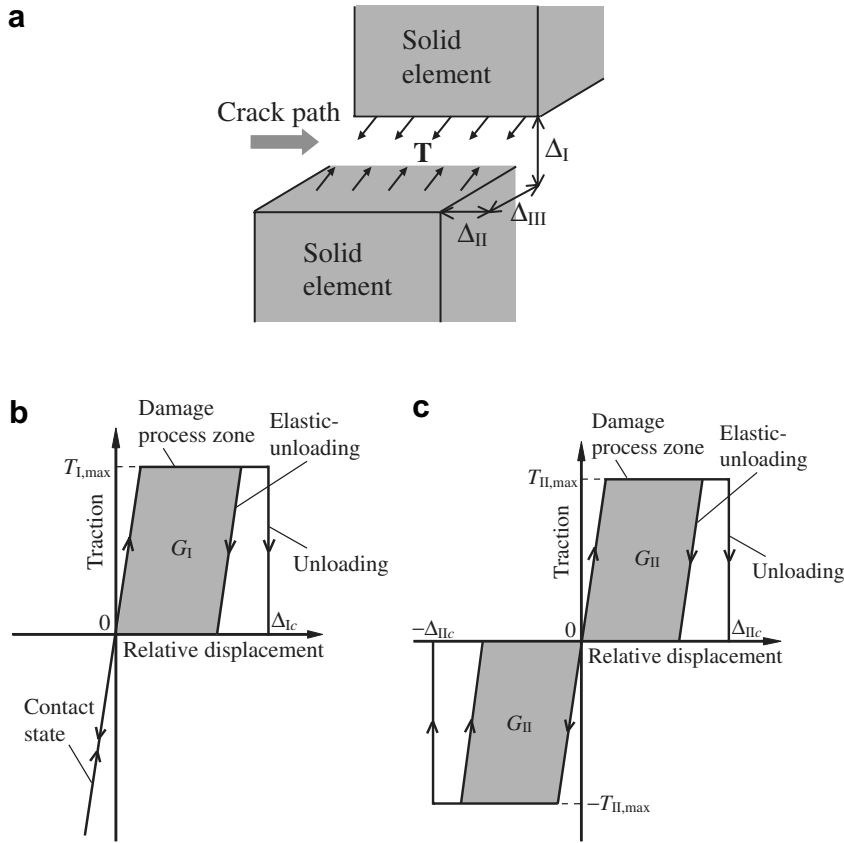
Fig. 5. Dugdale cohesive element used in the simulation: (a) cohesive element, (b) Mode-I cohesive law and (c) Mode-II and III cohesive law.

method becomes an indefinite matrix as the crack grows (Okabe et al., 2006). This is because the bi-linear cohesive elements employ a negative gradient to represent the relation between traction and relative displacement in the damage process. On the contrary, since the Dugdale cohesive element does not employ a negative gradient, the positive-definiteness of the tangent stiffness matrix can be easily ensured. The simulation with Dugdale cohesive element is thus less sensitive to the size of the finite element mesh than the bi-linear cohesive elements that include softening response in the damage process. This was demonstrated in our previous study. This is the reason for using the Dugdale cohesive element in the present study.

Since the Dugdale cohesive element is a two-parameter model (maximum traction and critical energy release rate), the brittle fracture of composites can be addressed by adjusting these parameters. Okabe et al. (2006) demonstrated for the transverse cracking problem in cross-ply laminates that the simulated results converge to the fracture mechanics results for brittle fracture, when the maximum traction of the cohesive element is increased.

Next, we present the formulation and solution strategy of the finite element simulation. The virtual work for the analytical region V including the cohesive zone S_{coh} is as follows.

$$\int_V \boldsymbol{\sigma} : \delta\mathbf{E}\,\mathrm{d}V + \int_{S_{\mathrm{coh}}} \mathbf{T} \cdot \delta\boldsymbol{\Delta}\,\mathrm{d}S = \int_{S_t} \mathbf{f} \cdot \delta\mathbf{u}\,\mathrm{d}S \tag{3}$$

Here, $\boldsymbol{\sigma}$ is the stress tensor, $\mathbf{E}$ is the Green–Lagrange strain tensor, $\mathbf{u}$ is the displacement vector, $\mathbf{f}$ is the external force vector on the prescribed boundary S_t, and δ is the virtual component. The second term of Eq. (3) corresponds to the virtual work by cohesive elements. Let us now consider the unknown variables at time $t' = t + \Delta t$, using the known variables until time t. Considering the limit $\Delta t \to 0$, Eq. (3) is linearized as

$$\Delta t \left(\int_V {}^t\dot{\boldsymbol{\sigma}} : \delta\mathbf{E}\, dV + \int_V {}^t\boldsymbol{\sigma} : (\delta\dot{\mathbf{E}})\, dV + \int_{S_{\text{coh}}} {}^t\dot{\mathbf{T}} \cdot \delta\boldsymbol{\Delta}\, dS \right) = \int_{S_t} {}^{t'}\mathbf{f} \cdot \delta\mathbf{u}\, dS - \int_V {}^t\boldsymbol{\sigma} : \delta\mathbf{E}\, dV - \int_{S_{\text{coh}}} {}^t\mathbf{T} \cdot \delta\boldsymbol{\Delta}\, dS$$

$$(4)$$

where $\cdot$ denotes the time derivative. This study uses the updated Lagrangian formulation to update the reference configuration for Eq. (4).

In Eq. (4), the constitution law of solid elements is given by

$$\dot{\boldsymbol{\sigma}} = \mathbf{C} : \dot{\mathbf{E}} \tag{5}$$

where $\mathbf{C}$ is the fourth-order tensor of the constitution law. In addition, the relation between traction $\mathbf{T}$ and relative displacement $\boldsymbol{\Delta}$ in Eq. (4) is represented as follows.

$$\dot{\mathbf{T}} = \mathbf{D}_{\text{coh}} \cdot \dot{\boldsymbol{\Delta}} \tag{6}$$

where

$$\mathbf{D}_{\text{coh}} = \begin{bmatrix} k_{t1} & 0 & 0 \\ 0 & k_n & 0 \\ 0 & 0 & k_{t2} \end{bmatrix} \quad \text{for } 0° \text{ ply crack} \tag{7}$$

$$\mathbf{D}_{\text{coh}} = \begin{bmatrix} k_{t1} & 0 & 0 \\ 0 & k_{t2} & 0 \\ 0 & 0 & k_n \end{bmatrix} \quad \text{for delamination} \tag{8}$$

where k_n, k_{t1}, and k_{t2} represent the gradients in the relation of cohesive elements in the normal (mode-I) and tangential (mode-II and III) directions.

$$\Delta t \left(\int_V \delta\mathbf{E} : ({}^t\mathbf{C} : {}^t\dot{\mathbf{E}})\, dV + \int_V {}^t\boldsymbol{\sigma} : (\delta\dot{\mathbf{E}})\, dV + \int_{S_{\text{coh}}} \delta\boldsymbol{\Delta} \cdot ({}^t\mathbf{T} \cdot {}^t\dot{\boldsymbol{\Delta}}) \cdot\, dS \right)$$
$$= \int_{S_t} {}^{t'}\mathbf{f} \cdot \delta\mathbf{u}\, dS - \int_V {}^t\boldsymbol{\sigma} : \delta\mathbf{E}\, dV - \int_{S_{\text{coh}}} {}^t\mathbf{T} \cdot \delta\boldsymbol{\Delta}\, dS \tag{9}$$

The following relationship can be obtained for the relative displacement $\boldsymbol{\Delta}$.

$$\delta\boldsymbol{\Delta} = \sum_{i=1}^{2m} \mathbf{L}^i \delta\mathbf{U}^i \equiv \mathbf{L}^e \delta\mathbf{U}^e \tag{10}$$

$$\dot{\boldsymbol{\Delta}} = \mathbf{L}^e \dot{\mathbf{U}}^e \tag{11}$$

where

$$\mathbf{L}^i = \begin{bmatrix} -N^i & 0 & 0 \\ 0 & -N^i & 0 \\ 0 & 0 & -N^i \end{bmatrix} \quad \text{for lower surface nodes} \tag{12}$$

$$\mathbf{L}^i = \begin{bmatrix} N^{i-m} & 0 & 0 \\ 0 & N^{i-m} & 0 \\ 0 & 0 & N^{i-m} \end{bmatrix} \quad \text{for upper surface nodes} \tag{13}$$

$$\mathbf{U}^i = \left\{ U_1^i \quad U_2^i \quad U_3^i \right\}^{\mathrm{T}} \tag{14}$$

where U is the nodal displacement, and the subscripts and superscripts for U are its direction and node number. The nodes on the lower surface of a cohesive element are numbered as 1 to m, and the nodes on the upper surface are numbered as $m+1$ to $2m$. The shape functions of typical two-dimensional isoparametric elements are used as the shape functions N^i ($i = 1, \ldots, m$).

Finally, Eq. (4) is discretized as

$$({}^{t}\mathbf{K} + {}^{t}\mathbf{K}_{\mathrm{coh}}) = {}^{t+\Delta t}\mathbf{F} - ({}^{t}\mathbf{Q} + {}^{t}\mathbf{Q}_{\mathrm{coh}}) \tag{15}$$

$${}^{t}\mathbf{K}_{\mathrm{coh}} = \sum_{e} \int_{S_{\mathrm{coh}}^{e}} \mathbf{L}^{e\mathrm{T}\,t}\mathbf{D}_{\mathrm{coh}}\mathbf{L}^{e}\,\mathrm{d}S \tag{16}$$

$${}^{t}\mathbf{Q}_{\mathrm{coh}} = \sum_{e} \int_{S_{\mathrm{coh}}^{e}} \mathbf{L}^{e\mathrm{T}\,t}\mathbf{T}\,\mathrm{d}S \tag{17}$$

where ${}^{t}\mathbf{K}$ and ${}^{t}\mathbf{K}_{\mathrm{coh}}$ are the tangential stiffness matrix of solid elements and cohesive elements, ${}^{t}\mathbf{Q}$ and ${}^{t}\mathbf{Q}_{\mathrm{coh}}$ are the nodal internal force vector of solid elements and cohesive elements, and ${}^{t+\Delta t}\mathbf{F}$ is the nodal external force vector. Eq. (15) is the basic equation of the simulation.

In order to consider the interaction of individual damage, we use the $R_{\min}$ method (Yamada et al., 1968) for solving Eq. (15). The $R_{\min}$ method is used to trace the assumed relation between relative displacement and traction of cohesive elements, as described below.

Step 1. (a) Check whether the traction at each integration point in the elastic region reaches its maximum value $T_{i,\max}$ ($i = \mathrm{I}, \mathrm{II}, \mathrm{III}$) (Fig. 6(a)).

(b) Check whether the energy-based criterion (Eq. (2)) is satisfied at each integration point in the damage process zone (Fig. 6(b)).

Step 2. When condition (a) or (b) is satisfied in Step 1, the integration point has the displacement increment past the corner points of the assumed relation. Thus, the ratio R of the displacement increment to return the corner point of the traction-relative displacement relation is calculated for each integration point. The integration point to give the minimum of R is then searched. By searching the integration point that is the first to reach the corner point in the increment, we can trace individual damage in proper sequence.

Step 3. When the integration point to give $R_{\min}$ satisfies condition (a), we reduce the displacement increment to the corner point and continues to the next increment without iterations. For condition (b), after reducing the displacement increment, we repeat the iterations with the time in Eq. (15) kept constant to eliminate the residuals generated by unloading the traction at the integration point of interest.
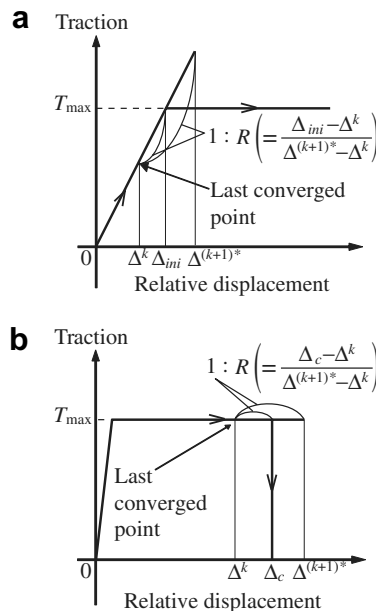

Fig. 6. $R_{\min}$ method applied to cohesive elements: (a) when the traction reaches its maximum value and (b) when the relative displacement reaches its critical value.

Based on this simulation procedure, we conduct a damage propagation simulation by applying a transverse load at the center of the laminate. It is expected that the stress gradient will become high near the applied force and in the damage process zone near the edge of the damage in this simulation. Therefore, it is necessary to divide these regions into fine meshes to ensure the accuracy of the finite element simulation.

For this purpose, this study proposes an efficient damage propagation simulation based on the updating-element technique. First, the analytical region is partitioned into a circular region including the propagated interlaminar delamination and the outer region, as shown in Fig. 7(a). Cohesive elements representing interlaminar delaminations are incorporated at the ply interfaces within the circular region. Cohesive elements representing a ply crack at the center of the lowermost 0° ply are also incorporated, as indicated in the figure. The circular region is divided into fine meshes with constant intervals, using 15-node triangle-pole solid elements and 20-node hexahedron solid elements. As the interlaminar delamination propagates, the radius r of the circular region is enlarged. In this simulation, the radius r is determined so that the edge of the circular region is 10 mm further from the edge of the interlaminar delamination. The outer region is then divided into 15-node triangle-pole elements. The mesh of the outer region can easily be coarsened while maintaining the accuracy of the analysis, with the use of Delaunay automatic mesh generation (Taniguchi, 1992; Nishioka et al., 2001). Since the finite element mesh is automatically adjusted to the increasing damage region during the incremental analysis, the proposed simulation can reduce computational costs, whereas the fixed-element model must set the fine mesh all over the expected damage region before analysis.

The mesh update rearranges the integration points during the analysis where the values of the variables, such as displacement and stress, must be preserved. To maintain consistency between the variables before and after the mesh update, the present simulation uses Lawson's searching algorithm (Taniguchi, 1992) to search the position (element and local coordinates) in the mesh before the update where each new integration point in the updated mesh corresponds. The simulation then transfers the variables at the searched position to those of the new integration point. In addition, since new cohesive elements are added in the circular region
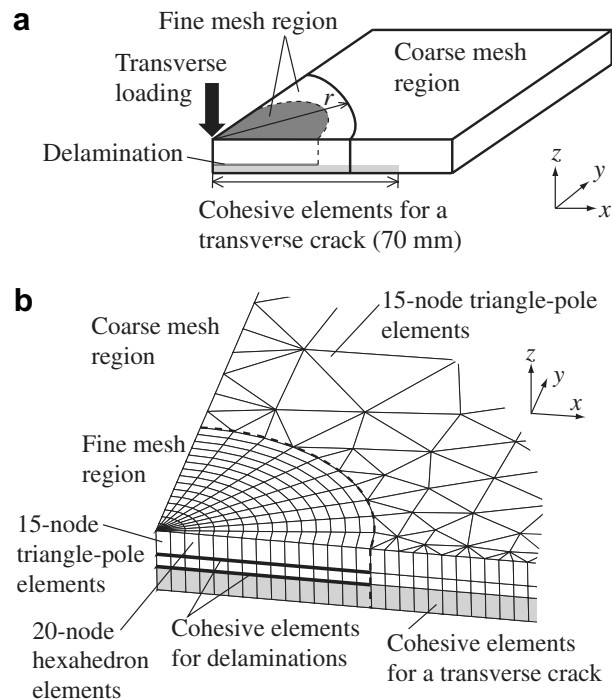

Fig. 7. Schematic of updating the model with an increasing damage region: (a) model partition into fine and coarse mesh regions and (b) finite element mesh near the fine mesh region.

after the mesh update, we substitute the stress at the corresponding position before the update into the traction at each integration point of the cohesive elements. Fig. 8 schematically illustrates this process.

4. Results and discussion

Based on the simulation procedure presented in the previous section, we simulated the propagation of interlaminar delamination in CFRP cross-ply laminates under transverse loading. Table 1 presents the material properties used in the simulation. These were reported by Yashiro et al. (2005). Table 2 lists the parameters of cohesive elements representing 0° ply crack and interlaminar delamination. As in the experiment, simply supported boundary conditions were applied at the circular edge, which was 35 mm
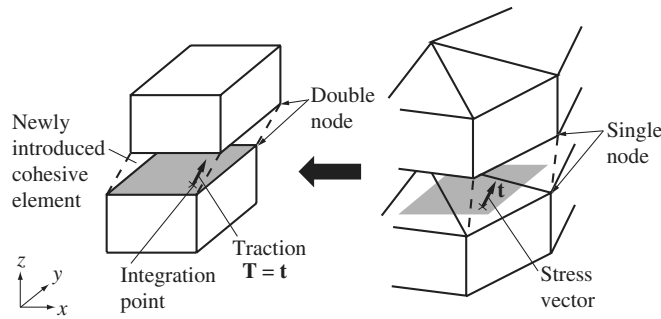

Fig. 8. Schematic of a newly added cohesive element by mesh update.

Table 1
Material properties of T800H/3631 unidirectional ply

Young's modulus	
E_{LL}	148 GPa
E_{TT}, E_{zz}	9.57 GPa
Poisson's ratio	
v_{LT}, v_{Lz}	0.356
v_{Tz}	0.49
Elastic shear modulus	
G_{LT}, G_{Lz}	4.5 GPa
G_{Tz}	3.5 GPa
Thermal expansion coefficient	
α_T, α_z	$36.0 \times 10^{-6}\,\mathrm{K}^{-1}$
α_L	$-0.6 \times 10^{-6}\,\mathrm{K}^{-1}$
Temperature change ΔT	165 K

Subscripts L, T, z denote the fiber axial direction, transverse direction and thickness direction, respectively.

Table 2
Strength parameters of cohesive elements used in the simulation

Ply crack	
Mode-I maximum traction $T_{\mathrm{I,max}}$	60 MPa
Mode-II, III maximum traction $T_{\mathrm{II,max}}$, $T_{\mathrm{III,max}}$	100 MPa
Mode-I critical energy release rate G_{Ic}	100 J/m²
Mode-II, III critical energy release rate G_{IIc}, G_{IIIc}	200 J/m²
Delamination	
Mode-I maximum traction $T_{\mathrm{I,max}}$	60 MPa
Mode-II, III maximum traction $T_{\mathrm{II,max}}$, $T_{\mathrm{III,max}}$	100 MPa
Mode-I critical energy release rate G_{Ic}	100 J/m²
Mode-II, III critical energy release rate G_{IIc}, G_{IIIc}	400 J/m²

in diameter. The simulation represented these boundary conditions by applying the penalty-function method to selected points with constant intervals. The analysis was controlled by the uniformly distributed transverse load, which was applied to the element at the center of the plate. (A similar treatment can be found in Li et al. (2002).)

The simulated results indicated that a ply crack first extended in the lowermost 0° ply and then the interlaminar delamination at the 90/0 ply interface was generated at the crack tip. Fig. 9 illustrates the simulated results of interlaminar delamination at the 90/0 ply interface at three levels of the applied transverse load. Each load level corresponds to the impact energy presented in Fig. 3. (The correspondence between load and impact energy was verified by a spring-mass model. A general explanation of the spring-mass model can be found in Shivakumar et al. (1985) and Olsson (1992).) The figure plots the distribution of D defined in Eq. (2). $D \approx 0$ denotes an intact interface, $0 \leqslant D \leqslant 1$ denotes a damage process zone, and $D \geqslant 1$ denotes a completely damaged interface. As also seen in Fig. 3, the interlaminar delamination is butterfly-shaped and extends longer in the 0° fiber direction. The delaminated area is enlarged with the increasing transverse loading. Although the minute difference in the delamination length in x-direction can be found between Figs. 3 and 9 due to the difference of the 0° ply crack growth, the simulated results agree well with experimental results as a whole.
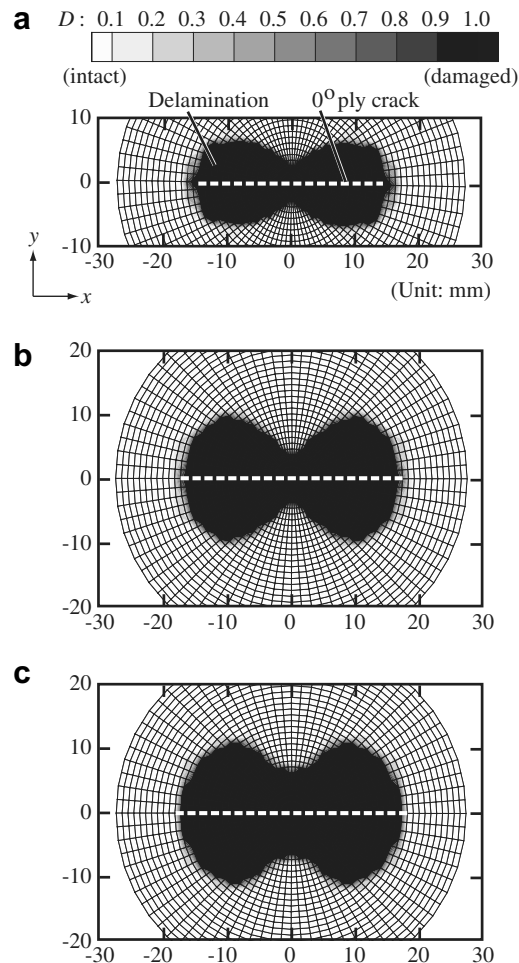

Fig. 9. Simulated delaminations at the 90/0 ply interface in CFRP cross-ply laminates: (a) after 1 J impact (impact force = 1.4 kN), (b) after 2 J impact (impact force = 2.3 kN) and (c) after 3 J impact (impact force = 3.0 kN).
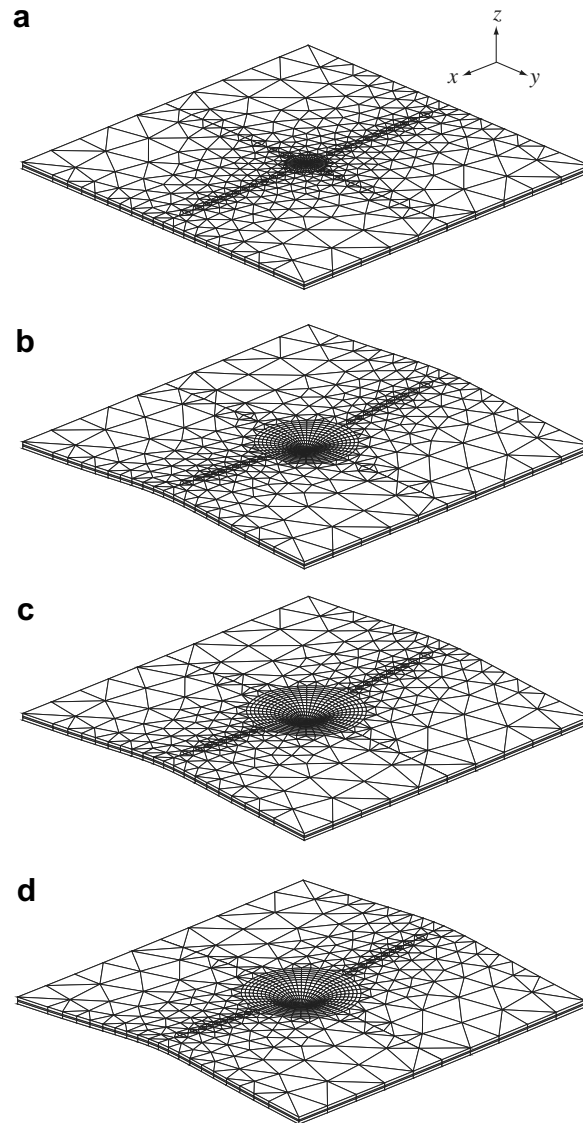
Fig. 10. Variations of the finite element mesh with increasing damage region: (a) initial mesh, (b) impact force = 1.3 kN, (c) impact force = 2.3 kN and (d) impact force = 3.0 kN.

As the interlaminar delamination increased, the finite element mesh was updated as shown in Fig. 10. Fig. 11 plots the variations of the computation time as the radius of the delaminated region increases. At the beginning of the damage propagation, the computation time could be significantly reduced, because the degree of freedom in the model was small. In addition, we conducted a similar damage propagation simulation using the *fixed*-element model depicted in Fig. 12, which was *not updated* during the analysis, for comparison. The number of degrees of freedom in the fixed-element model was 21,141, which was larger than the degrees of freedom (15,438) of Fig. 10(d). However, the simulated results could not reproduce the shape of interlaminar delamination, as presented in Fig. 13, since the fixed-element model did not set the fine-mesh region in the damage process zone. These results confirmed that the proposed simulation using the updating-element technique is superior to the fixed-element model, because it can reduce computational costs while maintaining accuracy in the damage process zone of interlaminar delamination.
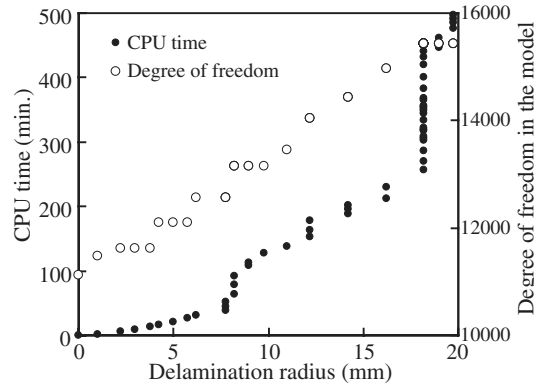
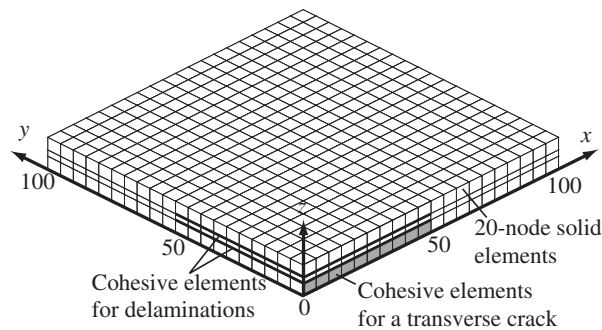Fig. 11. Variations of the computation time with increasing damage region.

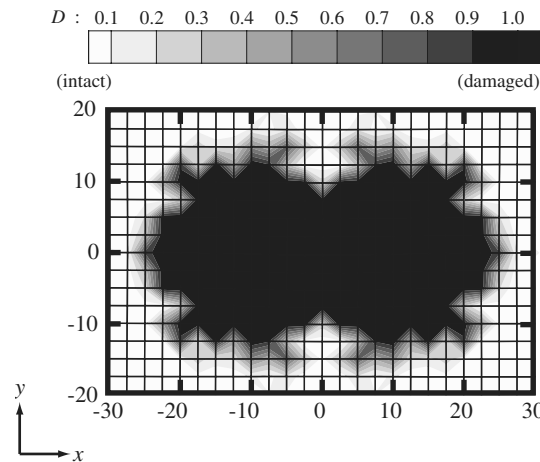Fig. 12. Fixed-element model used in the comparison.

Fig. 13. Simulated delamination in the fixed-element model (after 3 J impact).

5. Conclusions

This paper proposed a numerical simulation of interlaminar damage propagation in FRP cross-ply laminates under transverse loading, using the finite element method. The proposed simulation addresses the propagation of a ply crack and interlaminar delamination observed in the experiment, using the Dugdale cohesive element method consistent with the fracture mechanics method. In addition, we introduced a

simulation procedure using the updating-element method to analyze the damage process zone of internal damage with high accuracy. We demonstrated that the computation time can be reduced because the updating-element method can arbitrarily adjust the fine-mesh region to the damaged region. Moreover, the proposed simulation well reproduced the shape of interlaminar delamination in the laminates observed in the experiment, compared with the fixed-element model consisting of about the same degrees of freedom.

Acknowledgements

References

Abrate, S., 1991. Impact on laminated composite materials. Applied Mechanics Review 44, 155–191.

Alfano, G., Crisfield, M.A., 2001. Finite element interface models for the delamination analysis of laminated composites: mechanical and computational issues. International Journal for Numerical Methods in Engineering 50, 1701–1736.

Borg, R., Nilsson, L., Simonsson, K., 2004. Simulation of low velocity impact on fiber laminates using a cohesive zone based delamination model. Composites Science and Technology 64, 279–288.

Collombet, F., Labin, X., Lataillade, J.L., 1998. Impact behavior of laminated composites: physical basis for finite element analysis. Composites Science and Technology 58, 463–478.

Dugdale, D.S., 1960. Yielding of steel sheets containing slits. Journal of the Mechanics and Physics of Solids 8, 100–104.

Geubelle, P.H., Baylor, J.S., 1998. Impact-induced delamination of composites: a 2D simulation. Composites 29B, 589–602.

Johnson, A.F., Pickett, A.K., Rozycki, P., 2001. Computational methods for predicting impact damage in composite structures. Composites Science and Technology 61, 2183–2192.

Li, C.F., Hu, N., Yin, Y.J., Sekine, H., Fukunaga, H., 2002. Low-velocity impact-induced damage of continuous fiber-reinforced composite laminates. Part I. An FEM numerical model. Composites 33A, 1055–1062.

Liu, S., Kutlu, Z., Chang, F.K., 1993. Matrix cracking and delamination in laminated composite beams subjected to a transverse concentrated line load. Journal of Composite Materials 27, 436–470.

Nishioka, T., Tokudome, H., Kinoshita, M., 2001. Dynamic fracture-path prediction in impact fracture phenomena using moving finite element method based on Delaunay automatic mesh generation. International Journal of Solids and Structures 38, 5273–5301.

Okabe, T., Nishikawa, M., Takeda, N., 2006. Numerical simulation of tensile damage process in FRP cross-ply laminates. Transactions of the Japan Society of Mechanical Engineers Series A 72, 1254–1261 (in Japanese).

Olsson, R., 1992. Impact response of orthotropic composite plates predicted from a one-parameter differential equation. AIAA Journal 30, 1587–1596.

Shivakumar, K.N., Elber, W., Illg, W., 1985. Prediction of impact force and duration due to low-velocity impact on circular composite laminates. Transactions of the ASME: Journal of Applied Mechanics 52, 674–680.

Taniguchi, T., 1992. Automatic Mesh Generation for FEM: Use of Delaunay Triangulation. Morikita Publishing (in Japanese).

Yamada, Y., Yoshimura, N., Sakurai, T., 1968. Plastic stress–strain matrix and its application for the solution of elastic–plastic problems by the finite element method. International Journal of Mechanical Sciences 10, 343–354.

Yashiro, S., Takeda, N., Okabe, T., Sekine, H., 2005. A new approach to predicting multiple damage states in composite laminates with embedded FBG sensors. Composites Science and Technology 65, 659–667.